

Intrinsic supercurrent non-reciprocity coupled to the crystal structure of a van der Waals Josephson barrier

Jae-Keun Kim^{1*}, Kun-Rok Jeon², Pranava K. Sivakumar¹, Jaechun Jeon¹, Chris Koerner³,

Georg Woltersdorf³ and Stuart S. P. Parkin^{1*}

¹*Max Planck Institute of Microstructure Physics, Weinberg 2, 06120 Halle (Saale), Germany*

²*Department of Physics, Chung-Ang University (CAU), Seoul 06974, Republic of Korea*

³*Department of Physics, Martin Luther University Halle-Wittenberg, Von-Danckelmann-Platz 3, 06120 Halle, Germany*

*To whom correspondence should be addressed: jkkim@mpi-halle.mpg.de;

stuart.parkin@mpi-halle.mpg.de

Non-reciprocal electronic transport in a spatially homogeneous system arises from the simultaneous breaking of inversion and time-reversal symmetries. Superconducting and Josephson diodes, a key ingredient for future non-dissipative quantum devices, have recently been realized. Only a few examples of a vertical superconducting diode effect have been reported and its mechanism, especially whether intrinsic or extrinsic, remains elusive. Here we demonstrate a substantial supercurrent non-reciprocity in a van der Waals vertical Josephson junction formed with a T_d -WTe₂ barrier and NbSe₂ electrodes that clearly reflects the intrinsic crystal structure of T_d -WTe₂. The Josephson diode efficiency increases with the T_d -WTe₂ thickness up to critical thickness, and all junctions, irrespective of the barrier thickness, reveal magneto-chiral characteristics with respect to a mirror plane of T_d -WTe₂. Our results, together with the twist-angle-tuned magneto-chirality of a T_d -WTe₂ double-barrier junction, show that two-dimensional materials promise vertical Josephson diodes with high efficiency and tunability.

The non-reciprocal behavior in dissipative current flows, known as the diode effect, has played a central role in modern electronic devices and circuits^{1,2}. In conventional schemes, non-reciprocity along the current direction arises from spatial inhomogeneity^{1,2}. Recently, it has been shown that when inversion and time-reversal symmetries are both broken, and in combination with a spin-orbit interaction (SOI), even spatially homogeneous systems can provide for diode functionality³⁻⁵. By implementing this magneto-chirality with superconductors (SCs) and matching the superconducting gap with the SOI energy^{6,7}, one can achieve a directional, non-dissipative, supercurrent flow, which is a prerequisite for the realization of future superconducting quantum devices. To date, several methods have been developed to intrinsically and/or extrinsically break the inversion symmetry. For example, via ionic-liquid gating of two-dimensional (2D) MoS₂ flakes, via the formation of non-centrosymmetric V/Nb/Ta superlattices or using a few layers of 2H-NbSe₂ have enabled the observation of non-reciprocal critical currents near their corresponding superconducting transition temperatures T_c ⁸⁻¹⁰. Notably, non-reciprocity in Josephson supercurrents have also been realized in lateral Josephson junctions (JJs) with structures: Al/InAs 2D electron gas (2DEG)/Al⁷, Nb/proximity-magnetized Pt/Nb¹¹ and Nb/NiTe₂ type-II Dirac semimetal/Nb¹². To break the inversion symmetry, the first two utilize a Rashba(-type) superlattice and barrier, respectively, whereas the last exploits topological surface states in a NiTe₂ barrier. Very recently, a field-free Josephson diode effect has been observed in vertical NbSe₂/Nb₃Br₈/NbSe₂ junctions¹³, but the non-reciprocal supercurrents appear in the direction along which the inversion symmetry is broken and the diode polarity is, moreover, independent of an applied magnetic field, making investigations of other devices highly desirable to unravel the role of van der Waals barriers.

Here, we utilize T_d -WTe₂ single-crystal exfoliated flakes as an inherently inversion symmetry breaking barrier in van der Waals (vdW) JJs and through extensive measurements of the T_d -WTe₂ flake thickness, magnetic field strength/angle and temperature dependences, we demonstrate that the supercurrent non-reciprocity along the vertical direction is intimately connected and is highly dependent on the crystal structure of the T_d -WTe₂ barrier, thereby allowing a clear distinction between intrinsic and extrinsic mechanisms^{7,11,12}. Our study establishes that the *co-existence* of the magneto-linearity, the magneto-chirality and the thickness and temperature-scaleable diode efficiency constitute the *intrinsic* supercurrent non-reciprocity, coupled to the crystal structure of a vdW barrier.

As illustrated in Fig. 1a, we fabricate vdW vertical JJs, in which a T_d -WTe₂ flake (2–60 nm thick) is sandwiched between two superconducting $2H$ -NbSe₂ flakes, in an inert atmosphere glovebox using dry transfer techniques (see Methods for details). Here, we employed NbSe₂ flakes thicker than 10 nm (16–17 \times the monolayer thickness) to preclude the unintended contribution of Ising Cooper pairing¹⁴ to the non-reciprocal transport properties of WTe₂ JJs. Note that T_d -WTe₂ itself exhibits highly interesting physical properties including a type-II Weyl semi-metallic behavior¹⁵, higher-order topological hinge states¹⁶ and quantum spin-Hall edge states¹⁷. In the present study, we focus on how the crystal inversion symmetry of T_d -WTe₂ is reflected in a vertical Josephson diode effect. Due to the lack of a screw rotational symmetry in T_d -WTe₂ from the Te atoms, the orthorhombic phase T_d -WTe₂ is non-centrosymmetric^{16,18,19}. The mirror-symmetry plane of T_d -WTe₂ along the b -axis (green plane in Fig. 1b) creates a polar axis, that is, an internal crystal electric field ϵ_{cr} ¹⁸ and together with the heavy W atoms provide a strong SOI. This, in conjunction with an external in-plane (IP) magnetic field $\mu_0 H_{\parallel}$, that breaks the time reversal symmetry, allows for an anomalous phase φ_0 to be created in the current-phase relationship (CPR) of the vertical JJ²⁰⁻²². As previously discussed theoretically (19-21), the presence of a finite φ_0 is essential to generate a rectified Josephson supercurrent, namely, unequal positive and negative Josephson supercurrents $I_c^+ \neq I_c^-$ ^{7,11}.

Below, we will separate a crystal-asymmetry-driven intrinsic diode effect from other extrinsic possibilities in the following manner. When the dc bias current I is applied along the vertical direction ($\parallel c$ -axis) and the IP magnetic field is applied in the a - b plane of the WTe₂ (blue plane in Fig. 1b), the Josephson diode efficiency $\eta = \frac{I_c^+ - |I_c^-|}{I_c^+ + |I_c^-|}$ is given by $\eta \propto \varphi_0 \propto \mu_0 H_{\parallel} \cdot \sin(\theta_{MC})$. Here θ_{MC} is the relative angle between the polar axis ($\parallel b$ -axis) of WTe₂ and the applied $\mu_0 H_{\parallel}$ ^{7,20-22}. The magneto-linearity ($\propto \mu_0 H_{\parallel}$) and the magneto-chirality [$\propto \sin(\theta_{MC})$] of η are key measures of the intrinsic Josephson diode effect.

Figure 1c displays representative current-voltage (I - V) curves for a NbSe₂/ T_d -WTe₂/NbSe₂ vdW JJ formed with a 23-nm-thick T_d -WTe₂ barrier. I - V curves are shown when $\mu_0 H_{\parallel} = 0$ (black), +6 (orange) and –6 (green) mT are applied at a fixed $\theta_{MC} \approx 86.6^\circ$ ($\theta = 45^\circ$). These measurements are performed below the junction's $T_c \approx 5$ K. θ is the angle of $\mu_0 H_{\parallel}$ relative to an edge of the Si wafer on which the exfoliated layers were placed: the wafer had been cut into a rectangular shape

to define a clear reference direction. It is clear that a critical current asymmetry ($\Delta I_c = I_c^+ - |I_c^-| \neq 0$) is only developed when $\mu_0 H_{\parallel}$ is non-zero and that the polarity of ΔI_c is inverted when the direction of $\mu_0 H_{\parallel}$ is reversed. These features correspond to a Josephson diode effect.

The magneto-linearity of η ($\propto \mu_0 H_{\parallel}$) is first checked by measuring how I_c^+ and $|I_c^-|$ vary with the strength of $\mu_0 H_{\parallel}$ for a fixed $\theta_{MC} \neq 0^\circ$ ($\theta = 0^\circ$). From a comparison of $|I_c(\mu_0 H_{\parallel})|$ and $\eta(\mu_0 H_{\parallel})$ for several values of the thickness of WTe₂ (2, 7, and 60 nm) (Fig. 2, a-f), three notable features are revealed. First, for all the JJs, η increases linearly with increasing $\mu_0 H_{\parallel}$ up to a certain critical field, above which η starts to decay (Fig. 2, d-f). Second, when this field coincides with the first-order minimum field of the Fraunhofer interference pattern, η decays in a complex way with an accompanying sign change (Fig. 2, b and c, e and f). Third, the slope of the low-field $\eta(\mu_0 H_{\parallel})$ data (Fig. 2, d-f) depends critically on the orientation of the polar axis of the WTe₂ with respect to the applied $\mu_0 H_{\parallel}$. While the first and second features are qualitatively similar to previous studies on Al/2DEG/Al⁷ and Nb/NiTe₂/Nb¹² lateral JJs, the third, signifying the magneto-chirality of η [$\propto \sin(\theta_{MC})$], is a new finding from the NbSe₂/WTe₂/NbSe₂ vertical JJs. Note that no signature of fast oscillations, often attributed to topological edge states of WTe₂²³, are detected in measurements of the magnetic-field interference patterns for our vertical JJs (Fig. 2a-c). This is in agreement with theoretical considerations that topological edge states, that reside on the *a-b* planes of WTe₂²⁴, may contribute to lateral transport^{25,26} but not to vertical transport. This indicates the crystallographic origin of the WTe₂ barrier for the magneto-chirality that we report here.

To confirm this distinctive magneto-chirality, the $\mu_0 H_{\parallel}$ angular dependence of η is measured for each JJ. Note that this measurement is conducted in the low-field regime where the magneto-linearity of η ($\propto \mu_0 H_{\parallel}$) holds (see Fig. 2, d-f). As summarized in Fig. 3, a-c, the measured $\eta(\theta)$ data are all well fitted by a sine function, suggesting a magneto-chiral origin of the Josephson diode effect in the vdW WTe₂ JJs. Furthermore, there exists a visible shift between the sine fits to the $\eta(\theta)$ data for different WTe₂ JJs. This indicates that the crystal structure of the WTe₂ barrier indeed governs the Josephson supercurrent non-reciprocity in our system. The magneto-chirality described above predicts η to be maximized (minimized) when the applied $\mu_0 H_{\parallel}$ is aligned along the *a*-axis (*b*-axis). To identify the *a*- and *b*-axis of each WTe₂ barrier in the fabricated junctions, angle-resolved polarized Raman spectroscopy was carried out: this technique can readily characterize the crystal orientation of low-dimensional materials^{16,18}. Figure 3, d-f, show the

polarization angle dependent relative intensities of two distinct Raman peaks at $\sim 160 \text{ cm}^{-1}$ and $\sim 210 \text{ cm}^{-1}$. The extracted a - and b -axis of the WTe_2 from the Raman data (Fig. 3, d-f, see Supplementary Information S3 for the detailed analysis) agree with those from the $\eta(\theta)$ data (Fig. 3, a-c). These results strongly support an intrinsic-crystal-structure-reflected vertical Josephson diode effect. For completeness, we also fabricated and measured control vdW JJs, where the non-centrosymmetric WTe_2 barrier is replaced with a *centrosymmetric*²⁷ $1T'$ - MoTe_2 barrier. In addition, the effect of direct tunneling between the top and bottom superconducting NbSe_2 electrodes in JJs without any vdW- WTe_2 (Supplementary Information S6) were fabricated. None of the magnetolinerarity and the magneto-chirality effects are found in these experiments (see Supplementary Information S4), thereby pinpointing the critical role of the Josephson barrier's crystal structure for the supercurrent non-reciprocity in our WTe_2 JJs.

The proportionality of φ_0 to the barrier length is another characteristic feature of the intrinsic Josephson diode effect²⁰⁻²², so one can anticipate that the thicker the WTe_2 barrier, the greater the diode efficiency. To test this, we next investigate how the field-strength-normalized diode efficiency $\eta^* = \frac{\eta}{\mu_0 H_{\parallel}}$, measured at $\theta_{\text{MC}} = 90^\circ$, scales with the WTe_2 thickness (Fig. 4a). Note that since $\eta \propto \mu_0 H_{\parallel}$ in the low-field regime, η^* ($= \frac{\eta}{\mu_0 H_{\parallel}}$) allows for a more quantitative comparison. As the WTe_2 thickness is increased from 2 to 23 nm, we find that η^* increases linearly. This linear scaling behavior is, in fact, predicted theoretically for a ballistic JJ²⁰. When the thickness of the WTe_2 is increased to 60 nm, which is larger than the coherence length ($\sim 30 \text{ nm}$, Supplementary Information S5) and the c -axis mean free path ($\sim 40 \text{ nm}$)²⁸, η^* deviates from the linear thickness dependence. Given the distinctively different barrier-thickness dependence of φ_0 on whether the junction is in the ballistic or diffusive regime, such a deviation is likely related to a ballistic-to-diffusive (long-junction) transition²⁰⁻²².

The temperature T dependent evolution of η^* , gives additional information about the intrinsic Josephson diode properties. Figure 4b shows the T/T_c -dependent η^* for several WTe_2 JJs. It is especially noteworthy that the $\eta^*(T/T_c)$ data can be well described by a $\sqrt{1 - \frac{T}{T_c}}$ function for $\frac{T}{T_c} \gtrsim \frac{1}{3}$, as predicted in several earlier theoretical studies²⁰⁻²². For $\frac{T}{T_c} < \frac{1}{3}$, η^* tends to saturate, which is qualitatively similar to recent related experiments^{7,10}. A very recent theory predicts a

rather complicated T -dependence of the superconducting diode effect in diffusive Rashba-type SCs²⁹ as the low- T limit diode efficiency is affected sensitively by structural disorder and impurity scattering. On the other hand, for Al/2DEG/Al ballistic JJs⁷, the field-strength-dependent supercurrent non-reciprocity is explained by considering contributions from first and second order harmonics in the JJ CPR. If we apply this analysis to our $\eta^*(T/T_c)$ data, both harmonics seem to become constant at $\frac{T}{T_c} < \frac{1}{3}$, as is consistent with the calculation in Ref. 7.

To further show the importance of our vertical JJ platform, that goes beyond recent studies⁷⁻¹², we have fabricated vertical JJs with a twisted WTe₂ double-barrier (Methods). Note that the twist angle θ_{twist} between two distinct WTe₂ layers uniquely forms an artificial polar axis of the entire Josephson barrier in a controllable manner (Extended Data Fig. 1). As summarized in Extended Data Fig. 2, the magneto-chirality of supercurrent non-reciprocity in such JJs is not only determined by the polar axis of the top WTe₂ but also by that of the bottom WTe₂, demonstrating a tunable magneto-chirality via twist-angle engineering and opens an avenue for the development of twistable³⁰ active Josephson diodes.

We have carefully fabricated vdW vertical JJs with an inherently inversion symmetry breaking T_d -WTe₂ barrier. It enables us to demonstrate the intrinsic Josephson non-reciprocity²⁰⁻²², namely, the crystal structure of the Josephson barrier governs overall properties of the Josephson diode, which is unprecedentedly achieved. We believe that our result help understand better the barrier's role in the realization of rectified Josephson supercurrents in vdW heterostructures¹³. Our approach can be extended to other low-dimensional, low-symmetric and twisted vdW systems³¹⁻³³ for accelerating the development of two-dimensional superconducting devices and circuits.

Methods

Device fabrication. The NbSe₂/WTe₂/NbSe₂ van der Waals (vdW) heterostructures (Fig. S1, a-d) were formed using standard dry transfer techniques. All the needed processes, including mechanical exfoliation, pick-up and dry transfer of the vdW flakes, were performed inside a nitrogen gas filled glovebox to prevent the flakes from oxidizing in ambient air. First, NbSe₂ (≥ 10 nm thick) and WTe₂ (2–60 nm thick) flakes were exfoliated on to a 300-nm-thick SiO₂/p++ Si substrate. Each of the flakes needed to form the heterostructure was chosen by optical microscopy

examination. The chosen flakes were picked up sequentially using a polycarbonate (PC) film coated dome-shaped polydimethylsiloxane (PDMS) stamp. The flakes were aligned one on top of each other and then the entire stack was released and then placed on top of a set of pre-patterned gold electrodes on a second 300-nm-thick SiO₂/p++ Si substrate. The release process was performed at 200 C°, after which the entire stack in the Si substrate was immersed in a chloroform solution to remove any PC residue. Using this fabrication process flow, we also prepared three distinct types of JJs: 1) a control vdW JJ, in which the non-centrosymmetric WTe₂ barrier^{16,18,19} is replaced by a *centrosymmetric*²⁷ 1T- MoTe₂ barrier (Supplementary Information S4), 2) a reference vdW JJ with *no* WTe₂ barrier (Supplementary Information S6), and 3) a twisted WTe₂ double-barrier JJ (Extended Data Fig. 1-2), where one WTe₂ is twisted in-plane relative to the other WTe₂. For the formation of the twisted WTe₂ double-barriers, we first identified the crystal orientation of two chosen WTe₂ flakes through their elongated shapes¹⁶ (which tends to be along the *a*-axis), and then carefully twisted and stacked one on top of the other to realize $\theta_{twist} \approx 90^\circ$. After completing the transport measurements, we finally confirmed the respective crystal orientations of the top and bottom WTe₂ flakes by a means of angle-resolved polarized Raman spectroscopy.

Electrical measurements. The current-voltage (*I-V*) curves of the fabricated NbSe₂/WTe₂/NbSe₂ vdW vertical Josephson junctions (JJs) were measured in a BlueFors dilution refrigerator or a Quantum Design Physical Property Measurement System with base temperatures of ~20 mK and ~1.8 K, respectively. The four-point *I-V* measurements were carried out using a Keithley 6221 current source and a Keithley 2182A nanovoltmeter. An external in-plane magnetic field ($\mu_0 H_{\parallel}$), that was needed to break the time-reversal symmetry, was applied within the *a-b* plane of the WTe₂ single crystalline barrier. Note that θ is the angle of $\mu_0 H_{\parallel}$ relative to one edge of the Si wafer on which the exfoliated layer stack was placed: the wafer had been purposely cut into a rectangular shape to define a clear reference direction. The typical Josephson penetration depth³⁴ of our junctions (of at least a few μm) is much larger than the WTe₂ thickness, so we can exclude orbital magnetic field effects (or Meissner demagnetizing supercurrents) as a possible extrinsic source for the Josephson diode effect in our JJs. We measured the field strength dependent diode signals

(Fig. 2, A-C) by applying $\mu_0 H_{\parallel}$ along a given θ direction. The angle dependent diode signals (Fig. 3, A-C) were measured at a constant $\mu_0 H_{\parallel}$ using a vector field magnet.

Atomic force microscopy. To characterize the thickness of each WTe₂ barrier, we conducted atomic force microscopy (AFM) measurements on the fabricated vdW vertical JJs. The measured AFM image and height of each WTe₂ barrier layer are shown together with the corresponding optical micrograph of the JJs in Fig. S1.

Data availability

The data used in this paper are available from the corresponding authors upon reasonable request.

References

- 1 Sze, S. M. & Kwok, K. N. in *Physics of Semiconductor Devices* (2006).
- 2 Neamen, D. A. *Semiconductor physics and devices : basic principles*. (McGraw-Hill, 2012).
- 3 Onsager, L. Reciprocal Relations in Irreversible Processes. I. *Phys. Rev.* **37**, 405-426 (1931).
- 4 Kubo, R. Statistical-Mechanical Theory of Irreversible Processes. I. General Theory and Simple Applications to Magnetic and Conduction Problems. *J. Phys. Soc. Japan* **12**, 570-586 (1957).
- 5 Rikken, G. L. J. A., Fölling, J. & Wyder, P. Electrical Magnetochiral Anisotropy. *Phys. Rev. Lett.* **87**, 236602 (2001).
- 6 Tokura, Y. & Nagaosa, N. Nonreciprocal responses from non-centrosymmetric quantum materials. *Nat. Commun.* **9**, 3740 (2018).
- 7 Baumgartner, C. *et al.* Supercurrent rectification and magnetochiral effects in symmetric Josephson junctions. *Nat. Nanotechnol.* **17**, 39-44 (2022).
- 8 Wakatsuki, R. *et al.* Nonreciprocal charge transport in noncentrosymmetric superconductors. *Sci. Adv.* **3**, e1602390 (2017).

- 9 Ando, F. *et al.* Observation of superconducting diode effect. *Nature* **584**, 373-376 (2020).
- 10 Bauriedl, L. *et al.* Supercurrent diode effect and magnetochiral anisotropy in few-layer NbSe₂. *Nat. Commun.* **13**, 4266 (2022).
- 11 Jeon, K.-R. *et al.* Zero-field polarity-reversible Josephson supercurrent diodes enabled by a proximity-magnetized Pt barrier. *Nat. Mater.* **21**, 1008-1013 (2022).
- 12 Pal, B. *et al.* Josephson diode effect from Cooper pair momentum in a topological semimetal. *Nat. Phys.* **18**, 1228-1233 (2022).
- 13 Wu, H. *et al.* The field-free Josephson diode in a van der Waals heterostructure. *Nature* **604**, 653-656 (2022).
- 14 Xi, X. *et al.* Ising pairing in superconducting NbSe₂ atomic layers. *Nat. Phys.* **12**, 139-143 (2016).
- 15 Armitage, N. P., Mele, E. J. & Vishwanath, A. Weyl and Dirac semimetals in three-dimensional solids. *Rev. Mod. Phys.* **90**, 015001 (2018).
- 16 Choi, Y.-B. *et al.* Evidence of higher-order topology in multilayer WTe₂ from Josephson coupling through anisotropic hinge states. *Nat. Mater.* **19**, 974-979 (2020).
- 17 Wu, S. *et al.* Observation of the quantum spin Hall effect up to 100 kelvin in a monolayer crystal. *Science* **359**, 76-79 (2018).
- 18 Kang, K., Li, T., Sohn, E., Shan, J. & Mak, K. F. Nonlinear anomalous Hall effect in few-layer WTe₂. *Nat. Mater.* **18**, 324-328 (2019).
- 19 Xu, S.-Y. *et al.* Electrically switchable Berry curvature dipole in the monolayer topological insulator WTe₂. *Nat. Phys.* **14**, 900-906 (2018).
- 20 Buzdin, A. Direct Coupling Between Magnetism and Superconducting Current in the Josephson φ_0 Junction. *Phys. Rev. Lett.* **101**, 107005 (2008).
- 21 Kanschelle, F., Tokatly, I. V. & Bergeret, F. S. Theory of the spin-galvanic effect and the anomalous phase shift φ_0 in superconductors and Josephson junctions with intrinsic spin-orbit coupling. *Phys. Rev. B* **92**, 125443 (2015).
- 22 Bergeret, F. S. & Tokatly, I. V. Theory of diffusive φ_0 Josephson junctions in the presence of spin-orbit coupling. *Europhys. Lett.* **110**, 57005 (2015).
- 23 Kononov, A. *et al.* One-Dimensional Edge Transport in Few-Layer WTe₂. *Nano Lett.* **20**, 4228-4233 (2020).
- 24 Soluyanov, A. A. *et al.* Type-II Weyl semimetals. *Nature* **527**, 495-498,(2015).

- 25 Chen, C.-Z. *et al.* Asymmetric Josephson effect in inversion symmetry breaking topological materials. *Phys. Rev. B* **98**, 075430 (2018).
- 26 Souto, R. S., Leijnse, M. & Schrade, C. Josephson Diode Effect in Supercurrent Interferometers. *Phys. Rev. Lett.* **129**, 267702 (2022).
- 27 Qian, X., Liu, J., Fu, L. & Li, J. Quantum spin Hall effect in two-dimensional transition metal dichalcogenides. **346**, 1344-1347 (2014).
- 28 Li, P. *et al.* Evidence for topological type-II Weyl semimetal WTe₂. *Nat. Commun.* **8**, 2150 (2017).
- 29 Ilić, S. & Bergeret, F. S. Theory of the Supercurrent Diode Effect in Rashba Superconductors with Arbitrary Disorder. *Phys. Rev. Lett.* **128**, 177001 (2022).
- 30 Ribeiro-Palau, R. *et al.* Twistable electronics with dynamically rotatable heterostructures. *Science* **361**, 690-693 (2018).
- 31 Novoselov, K. S., Mishchenko, A., Carvalho, A. & Castro Neto, A. H. 2D materials and van der Waals heterostructures. *Science* **353**, 6298 (2016).
- 32 Diez-Merida, J. *et al.* Magnetic Josephson Junctions and Superconducting Diodes in Magic Angle Twisted Bilayer Graphene. *Preprint at <https://arxiv.org/abs/2110.01067>* (2021).
- 33 Lin, J.-X. *et al.* Zero-field superconducting diode effect in small-twist-angle trilayer graphene. *Nat. Phys.* **18**, 1221-1227 (2022).
- 34 Barone, A. & Paterno, G. *Physics and Applications of the Josephson Effect* 2nd edn (John Wiley & Sons, 1982).

Acknowledgements

SSPP acknowledges funding from the Deutsche Forschungsgemeinschaft (DFG, German Research Foundation) – project no. 443406107, Priority Programme (SPP) 2244.

Author contributions

J.-K.K. and S.S.P.P conceived of and designed the experiments with the help of K.-R.J. J.-K.K. fabricated the van der Waals Josephson junctions and carried out the transport measurements with the help of K.-R.J, P.K.S. and J.J. J.-K.K performed the Raman measurement with the help of C.K. J.-K.K analyzed the data with the guidance of K.-R.J. J.-K.K., K.-R.J and S.S.P.P. wrote the

manuscript with input from all the other authors.

Additional information

Reprints and permissions information is available at www.nature.com/reprints. Correspondence and requests for materials should be addressed to J.-K.K or S.S.P.P.

Competing interests

The authors declare no competing financial interests.

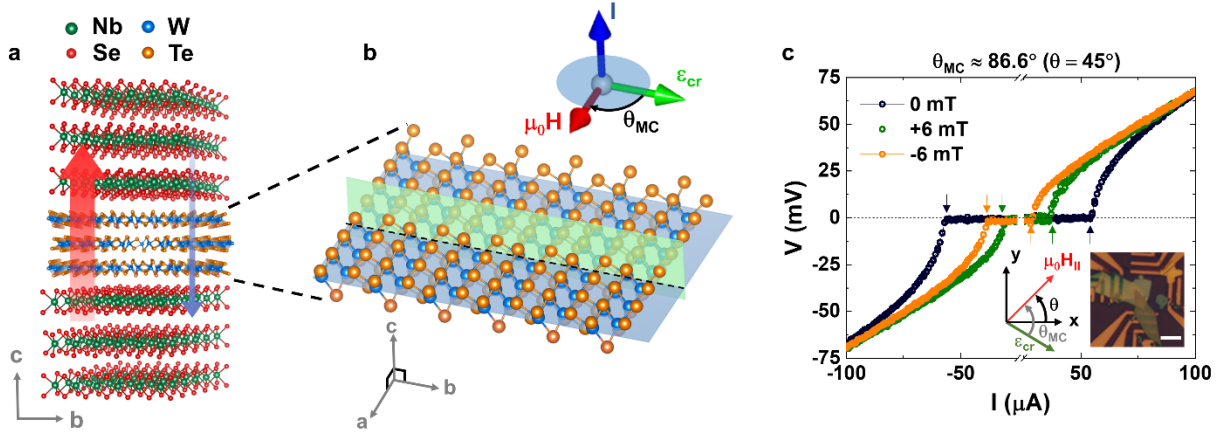


Fig. 1. Vertical rectified supercurrents in a van der Waals WTe₂ Josephson junction. **a**, Schematic of a NbSe₂/T_d-WTe₂/NbSe₂ van der Waals vertical Josephson junction (JJ). The combination of intrinsic inversion symmetry breaking within the T_d-WTe₂ barrier and time-reversal symmetry breaking by an applied magnetic field give rise to the (vertical) supercurrent non-reciprocity. **b**, Schematic diagram of the crystal structure of WTe₂. Orange (blue) symbols represent the W (Te) atoms. θ_{MC} is defined as the relative angle between the polar axis along *b*-axis, the mirror plane of T_d-WTe₂ (green plane), and the direction of the in-plane (IP) magnetic field $\mu_0 H_{||}$ applied within the *a*-*b* plane of T_d-WTe₂ (blue plane). **c**, Current-voltage *I*-*V* curves of a van der Waals JJ with a 23 nm thick T_d-WTe₂ barrier for $\mu_0 H_{||} = 0$ (black), +6 (orange) and -6 (green) mT. Note that θ is the angle of $\mu_0 H_{||}$ relative to an edge of the rectangular Si wafer on which the JJ was formed.

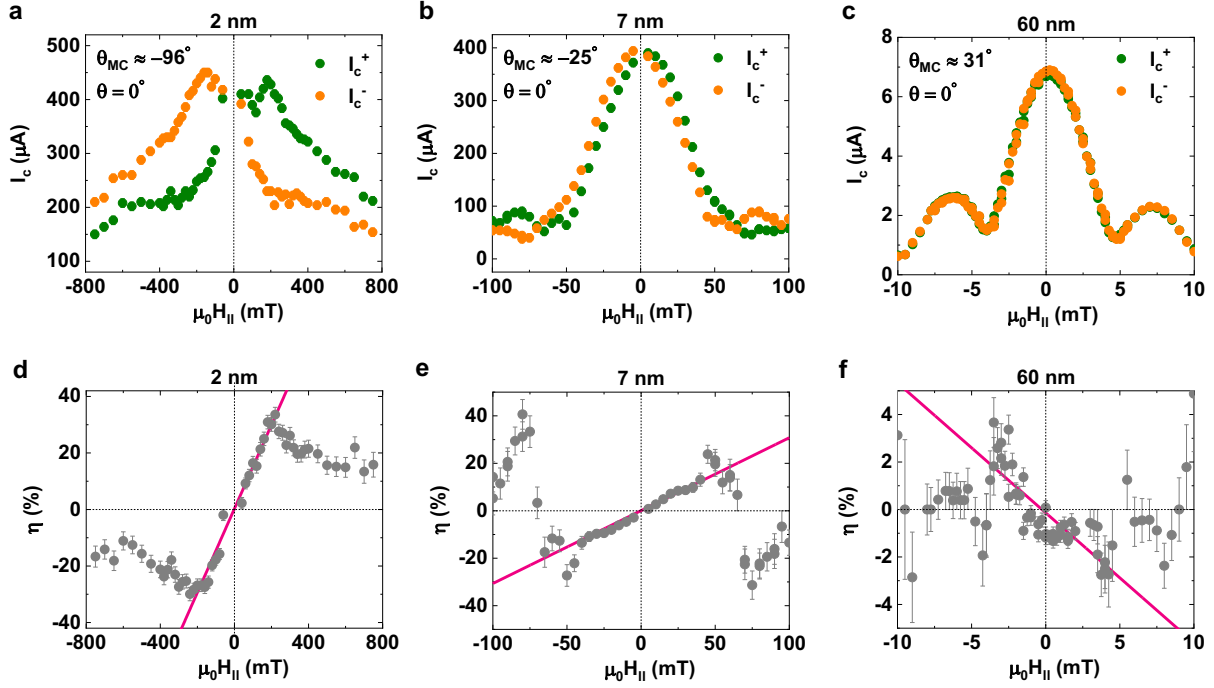


Fig. 2. Scaling of Josephson supercurrent non-reciprocity with magnetic field strength. **a, b, c,** Positive and negative Josephson critical current I_c^+ (green) and $|I_c^-|$ (orange) *versus* in-plane (IP) magnetic field $\mu_0 H_{\parallel}$ for **(a)** 2 nm, **(b)** 7 nm and **(c)** 60 nm thick T_d -WTe₂ barriers in a NbSe₂/ T_d -WTe₂/NbSe₂ Josephson junction. The measurement was conducted at $T = 200$ mK for the 2 nm and 7 nm thick junctions and $T = 20$ mK for the 60 nm thick junction, respectively. **d, e, f,** Josephson diode efficiency ($\eta = \frac{I_c^+ - |I_c^-|}{I_c^+ + |I_c^-|}$) as a function of $\mu_0 H_{\parallel}$ for **(e)** 2 nm, **(d)** 7 nm and **(f)** 60 nm thick T_d -WTe₂ barriers. Note that the pink fits indicate a linear scaling behavior of the diode efficiency with $\mu_0 H_{\parallel}$ up to a critical field, above which the diode efficiency drops.

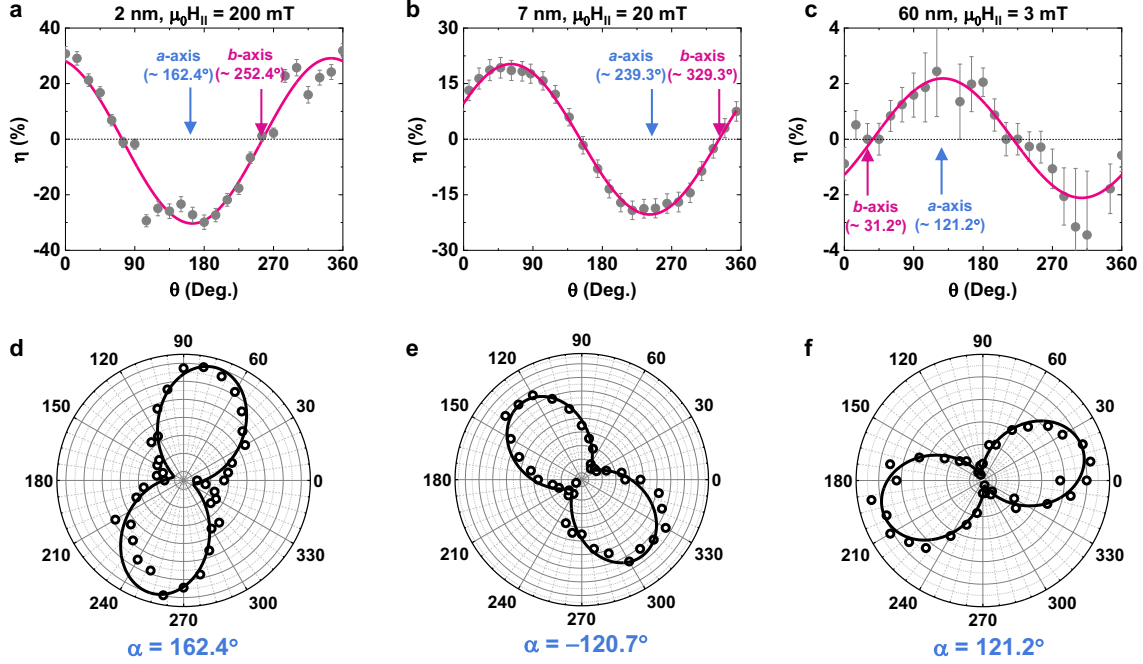


Fig. 3. Magneto-chiral angular dependence of the supercurrent non-reciprocity on the WTe_2 crystal structure. **a, b, c**, Field angle dependent Josephson diode efficiency ($\eta = \frac{I_c^+ - |I_c^-|}{I_c^+ + |I_c^-|}$) of $\text{NbSe}_2/T_d\text{-WTe}_2/\text{NbSe}_2$ junctions with **(a)** 2 nm, **(b)** 7 nm and **(c)** 60 nm thick $T_d\text{-WTe}_2$ barriers. Pink lines represent sine fits to the data. **d, e, f**, Polarization angle dependent relative intensity of two distinct Raman peaks (~ 160 cm^{-1} and ~ 210 cm^{-1}), from which the *a*- and *b*-axis of the WTe_2 can be determined. The *a*- and *b*-axis directions of the WTe_2 flake found in this way are indicated by arrows in **a, b, c**.

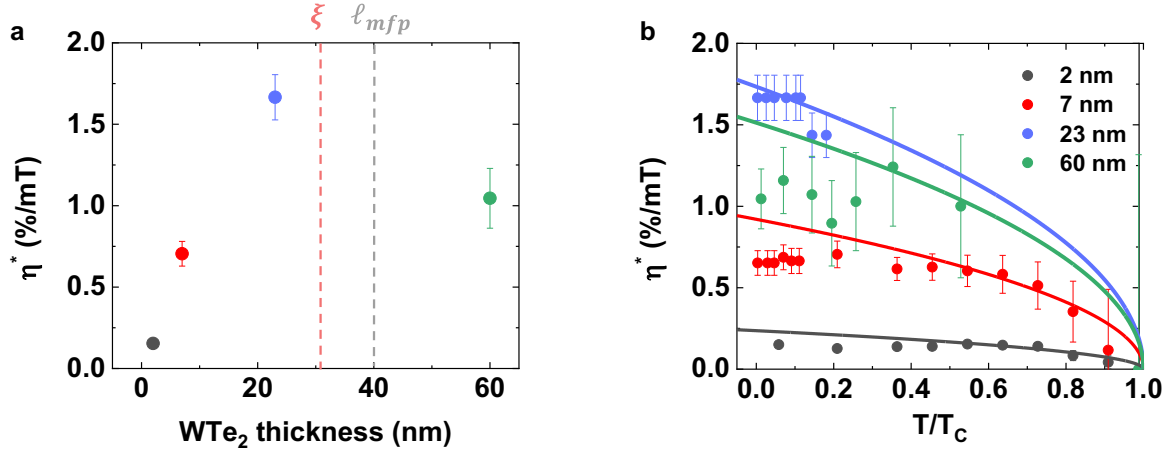
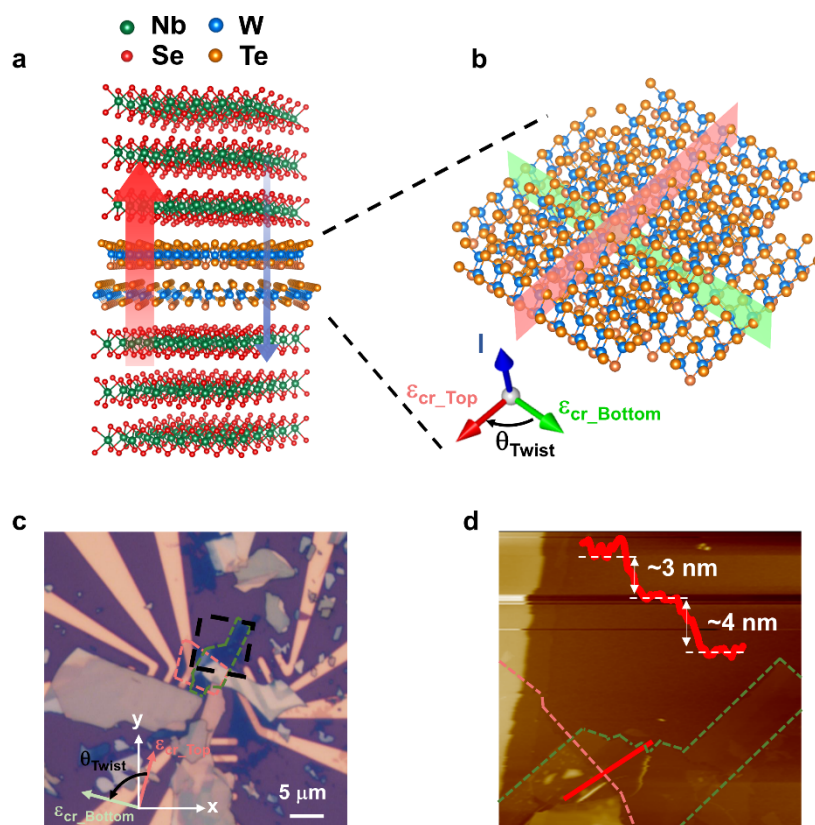


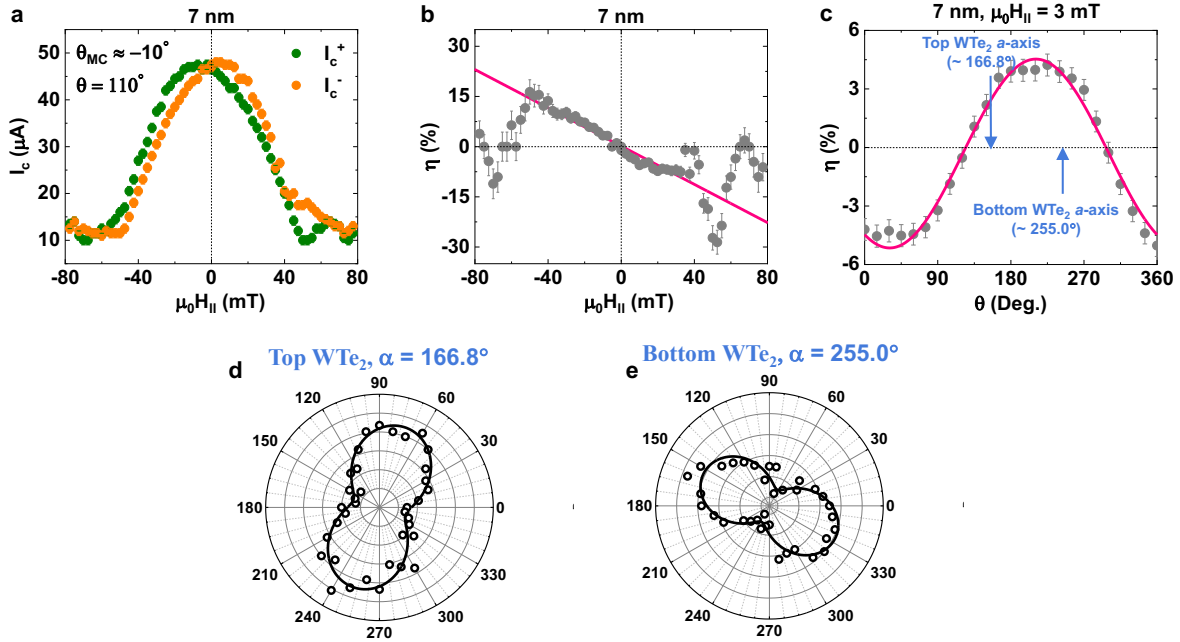
Fig. 4. Thickness and temperature dependent Josephson supercurrent non-reciprocity. a, Field-normalized Josephson diode efficiency η^* ($= \frac{I_c^+ - |I_c^-|}{I_c^+ + |I_c^-|} / \mu_0 H_{\parallel}$, measured at $\theta_{MC} = 90^\circ$) as a function of the T_d - WTe_2 barrier thickness. Vertical red and gray dashed lines correspond to the coherence length (Supplementary Information S4) and c -axis mean free path²² of the T_d - WTe_2 . **b,** Normalized dependence of η^* as a function of normalized temperature T/T_c of NbSe₂/ T_d - WTe_2 /NbSe₂ Josephson junctions with different T_d - WTe_2 barrier thicknesses (2, 7, 23 and 60 nm).

Solid lines represent fits to the data of $\sqrt{1 - \frac{T}{T_c}}$.

Extended Data Figures



Extended Data Figure 1. Fabrication of twisted WTe₂ double-barrier JJ **a**, Schematic diagram of a NbSe₂/twisted-WTe₂ double-barrier/NbSe₂ vdW vertical JJ. **b**, magnified schematic of the crystal structure of the twisted-WTe₂ double-barrier. Notably, the vector addition of the internal crystal fields ϵ_{cr_Top} and ϵ_{cr_Bottom} of the top and bottom WTe₂ layers, respectively, with the twist angle θ_{twist} leads to a new artificial polar axis of the entire Josephson barrier. **c**, Optical micrograph of the twisted-WTe₂ double-barrier JJ. The top (bottom) WTe₂ flake is marked by the red (green) dashed line. ϵ_{cr_Top} (ϵ_{cr_Bottom}) is defined to be along the polar axis (*b*-axis) of the top (bottom) WTe₂. These axes are directly probed by angle-resolved polarized Raman spectroscopy, as depicted on the optical micrograph. The black dashed box represents the area scanned by AFM as shown in **d**. **d**, AFM image of respective WTe₂ barriers. Inset: depth profile along the red solid line.



Extended Data Figure 2. Tuned magneto-chirality using the artificial polar axis of a twisted WTe₂ double-barrier JJ **a**, Positive and negative Josephson critical current I_c^+ (green) and $|I_c^-|$ (orange) *versus* in-plane (IP) magnetic field $\mu_0 H_{||}$ for twisted-WTe₂ double barrier JJ. Josephson diode efficiency $\eta (= \frac{I_c^+ - |I_c^-|}{I_c^+ + |I_c^-|})$ as a function of magnetic field strength **(b)** and angle **(c)** for the twisted WTe₂ double-barrier JJ. Polarization-angle-dependent relative intensity of two distinct Raman peaks ($\sim 160 \text{ cm}^{-1}$ and $\sim 210 \text{ cm}^{-1}$), from which one can determine the *a*- and *b*-axes of the top **(d)** and bottom **(e)** WTe₂ barriers. The measured *a*-axis directions of the top and bottom WTe₂ vdw layers are indicated by arrows in **c**. As can be seen in **c**, the magneto-chiral non-reciprocal supercurrents of the twisted-WTe₂ double barrier JJ are successfully controlled by twisting the top WTe₂ barrier relative to the bottom one.